Jacutingaite-family: A class of topological materials

F. Crasto de Lima,[1,*] R. H. Miwa,[2,†] and A. Fazzio[1,‡]

[1]*Brazilian Nanotechnology National Laboratory CNPEM, Caixa Postal 6192, 13083-970 Campinas, São Paulo, Brazil*

[2]*Instituto de Física, Universidade Federal de Uberlândia, Caixa Postal 593, 38400-902 Uberlândia, Minas Gerais, Brazil*

(Received 10 September 2020; accepted 9 December 2020; published 23 December 2020)

Jacutingate, a recently discovered Brazilian naturally occurring mineral, has been shown to be an experimental realization of the Kane-Mele topological model. In this paper we present a class of materials, M_2NX_3 (M = Ni, Pt, and Pd; N = Zn, Cd, and Hg; and X = S, Se, and Te), sharing jacutingaite's key features, i.e., high stability and a topological phase. By employing *first-principles* calculations we extensively characterize the energetic stability of this class while showing a common occurrence of the Kane-Mele topological phase. Here we present Pt-based materials surpassing jacutingaite's impressive topological gap and lower exfoliation barrier while retaining its stability.

DOI: 10.1103/PhysRevB.102.235153

The spin-orbit coupling (SOC) in condensed matter is accountable for the rise of many phenomena, for instance, topological phases [1], Rashba states [2], exotic spin textures [3], magnetic anisotropy [4], and spin-orbit torque transfer [5], to cite a few. Since the successful synthesis of graphene [6], two-dimensional (2D) materials with sizable SOC have been pursued as a platform for designing new electronic and spintronic devices [7–9] as well as for the discovery and confirmation of new physical phenomena. For instance, two-dimensional hexagonal lattices and SOC are the key ingredients to the manifestation of the quantum spin Hall (QSH) state as predicted by Kane and Mele [10].

Indeed, recent research addressing topological phases in low-dimensional systems has boosted the search for new two-dimensional materials with large SOC, for instance, the 2D MXenes [11,12] and Bi-based systems [13–15]. Other strategies have been proposed based on the incorporation of adatoms [16–21] and proximity effects [22–24] in order to strengthen the spin-orbit effects. However, most of these routes face some difficulties, namely, (i) structural metastability, (ii) stability against environment conditions (for instance, oxidation processes), (iii) difficulties for the experimental realization, and (iv) loss of 2D character due to the electronic interaction with a given substrate. Thus, new 2D materials with large SOC, which overcomes the hindrances above, are still quite desirable.

Jacutingaite (Pt_2HgSe_3), a naturally occurring mineral, discovered in Brazil by Cabral *et al.* [25] in 2008, has been gaining attention in the last few years. The large SOC and the honeycomb structure of Hg atoms make jacutingaite, in its monolayer form, a place for the manifestation of the Kane-Mele topological phase [26], whereas in its bulk form it has been predicted to host dual topology, being a weak topological insulator and a topological crystaline insulator [27–29]. Both topological phases, namely, Kane-Mele in monolayer Pt_2HgSe_3 and dual in bulk Pt_2HgSe_3, have been experimentally observed through scanning tunneling microscopy [30] and angle-resolved photoemission [31] measurements. Its atomic structure [Fig. 1(a)] can be viewed as the transition metal dichalcogenide (TMD) $PtSe_2$ with a 1T structural phase, where 1/4 of the chalcogenides are replaced by Hg. Besides being a naturally occurring mineral, which indicates its stability at geological pressures and temperatures, Pt_2HgSe_3 has been experimentally synthesized [30–33], as well as its counterpart Pd-based jacutingaitelike structure, Pd_2HgSe_3 [34]. Those findings suggest that further combinations of a 1T TMD host with high SOC elements may result in distinct quantum spin Hall insulators based on jacutingaitelike 2D structures.

In this paper, we present a large class of highly stable materials hosting QSH and Z_2-metallic phases based on the Kane-Mele model. We employ density functional theory simulations (see Supplemental Materials [35] and Refs. [36–45] therein) of the structural and electronic properties of M_2NX_3 compounds with M = Ni, Pd, and Pt; N = Zn, Cd, and Hg; and X = S, Se, and Te. Throughout the extensive analysis of phase diagrams based on MNX compounds, we present a well-grounded prediction of the energetic stability of jacutingaitelike M_2NX_3 structures. Electronic structure calculations reveal the emergence of topological phases, with SOC-induced (nontrivial) band gaps surpassing the one of jacutingaite. Further topological characterization reveals the trivial $\rightarrow$ nontrivial transition as a function of the chemical composition, X = S $\rightarrow$ Te. Finally, addressing the design of nanodevices, we have examined some key features of these jacutingaitelike structures, namely, the stability/behavior of the (i) topological gap as a function of the mechanical strain and the (ii) work function for the different M_2NX_3 combinations.

As shown in Fig. 1(a), the M_2NX_3 jacutingaitelike structures share the same backbone geometry of the 1T TMDs (MX_2), where the chalcogenide atoms (X) are partially replaced by transition metals (N), $MX_2 \rightarrow M_2NX_3$, resulting in buckled $N-M-N$ bonds. The N atoms form triangular lattices on the opposite sides of the MX_2 host, which in turn

*felipe.lima@lnnano.cnpem.br

†hiroki@ufu.br

‡adalberto.fazzio@lnnano.cnpem.br

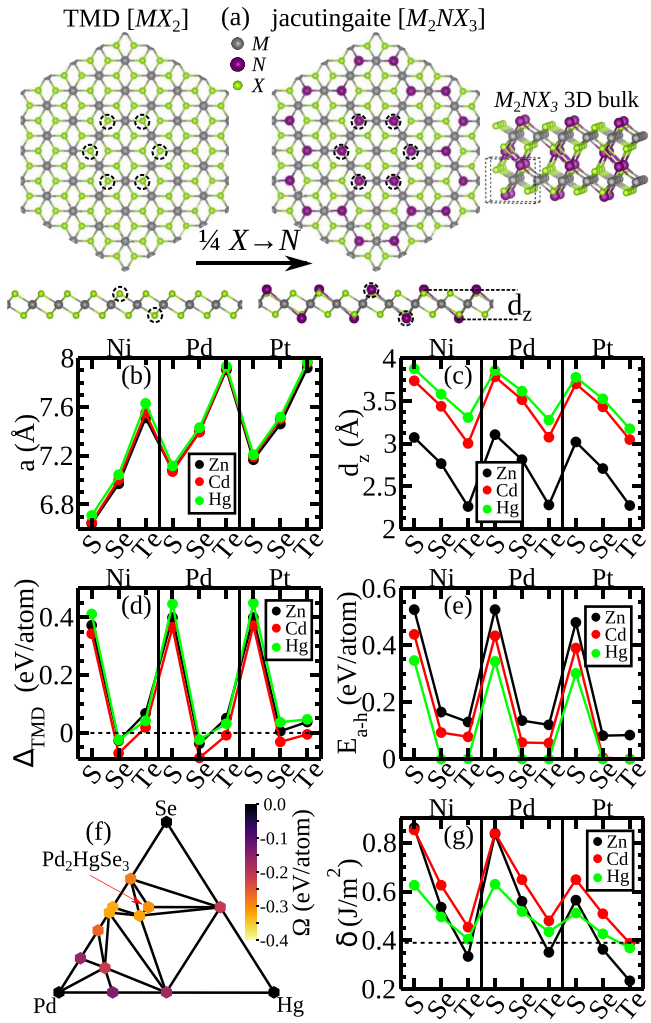

FIG. 1. (a) 2D TMD (MX_2) and 2D and 3D M_2NX_3 atomic structure, (b) lattice parameter, (c) bucking distance, (d) formation energy comparison between the TMD and M_2NX_3, (e) ternary MNX energy above hull for M_2NX_3, (f) convex hull for Pd_2HgSe_3, and (g) cleavage energy with the dashed line indicating the graphite cleavage barrier.

are rotated by 60° with respect to each other, giving rise to a buckled hexagonal lattice. At the equilibrium geometry, the lattice constants of the M_2NX_3 structures are practically independent of the transition metal, i.e., nearly the same as those of the hosts (MX_2). For instance, the equilibrium lattice constants of Pt_2NSe_3, for N = Zn, Cd, and Hg, differ by less than 0.9%, compared with that of 1T $PtSe_2$. Such independence is due to the $N-M-N$ buckled structure [Fig. 1(a)] acting as a source of strain relief induced by the foreign (N) atom. As shown in Fig. 1(c), the vertical buckling (d_z) of the $N-M-N$ bonds presents larger (lower) values for X = S (Te).

The energetic stability of the jacutingaitelike structures can be examined by comparing the formation energy of M_2NX_3 with the one of its respective (energetically stable) MX_2 host, $\Delta_{TMD} = \Omega[M_2NX_3] - \Omega[MX_2]$ [Fig. 1(d)]. Here the formation energy is given by a total energy difference between the compound x final system ($E[x]$) and the upper limit of the chemical potentials of its isolated compounds (μ^{bulk}), namely,

$$\Omega[x] = E[x] - \sum_i n_i \mu_i^{bulk},$$

where n_i indicates its number of atoms of the species $i = M$, N, and X. Our Δ_{TMD} results reveal that the jacutingaitelike structures are quite likely to occur for X = Se and Te. Here, we found negative values of Δ_{TMD} for the former, while for X = Te it increases by less than 0.1 eV/atom [Fig. 1(d)]. Meanwhile, for X = S the M_2NX_3 structure is less stable than that of its host by about 0.4 eV/atom.

Further structural stability of the jacutingaitelike M_2NX_3 structures has been examined through convex energy hull analysis, comparing their formation energies (Ω) with other MNX ternary phases extracted from the Materials Project database [43,46,47]. We found M_2NX_3 compounds being a node point in the convex hull (zero energy above the convex hull, $E_{a\text{-}h} = 0.0$ eV/atom [35]) showing its experimental stability [Fig. 1(e)]. For instance, in Fig. 1(f), Pd_2HgSe_3 lies in a convex node with a formation energy of −0.18 eV/atom. Additionally, all M_2HgSe_3 (M = Ni, Pd, and Pt) have $E_{a\text{-}h} =$ 0.0, as well as Pd_2HgTe_3, Pt_2CdTe_3, and Pt_2HgTe_3. For the Se- and Te-based materials that have nonzero energy above the hull we found $E_{a\text{-}h} < 0.18$ eV/atom, which indicates its high stability [48]. For instance, taking Pt_2ZnTe_3 as a case of study ($E_{a\text{-}h} = 0.08$ eV/atom), we have calculated its monolayer phonon dispersion [35], where its dynamical stability was confirmed by the absence of negative frequencies. Additionally, for the higher $E_{a\text{-}h}$ systems, X = S-based compounds, their negative values of formation energies, $\Omega < 0$ [35], indicate that they can be experimentally stabilized throughout specific synthesis routes and/or substrate support. Although the SOC has a stabilizing role in the jacutingaite phonon dispersion [26], we see that it changes the formation energy by ∼7 meV/atom, which does not change our conclusions.

The cleavage energy (δ) [49] is another important piece of structural information for the top-down synthesis of 2D systems. We found that the M_2NX_3 bulk phase presents cleavage energies in the range of other experimentally exfoliated materials [50]. For instance, jacutingaite has a cleavage energy, $\delta = 0.46$ J/m^2 comparable with that of graphene exfoliated from graphite, $\delta = 0.39$ J/m^2 [dashed line in Fig. 1(g)] [51]. When we compare the calculated cleavage energy and the vertical buckling of the $N-M-N$ bonds [d_z in Fig. 1(c)], it is noticeable that (i) for a given transition metal pair M-N the δ is proportional to d_z, being larger for X = S and lower for X = Te, this is in agreement with Ref. [32], where the authors verified that the N atoms are responsible for the interplane bound of the M_2NX_3 system, as shown in Fig. 1(a) for the M_2NX_3 3D structure. Indeed, taking the Cd and Hg systems, which have a similar bucking distance, the former presents a stronger interlayer bond ruled by the bonding energy of Cd-X being ∼60% greater than that of Hg-X. By contrast, for Zn, given its lower buckling distance, an interplay between the van der Waals interaction (of the TMD host) and the Zn interlayer chemical bond is present. The former dominates for lower d_z, leading to a weaker interlayer bond. (ii) For X = Te and N = Zn, the cleavage energy is always lower than that of graphene, where (iii) the cleavage energy of Pt_2HgTe_3 is

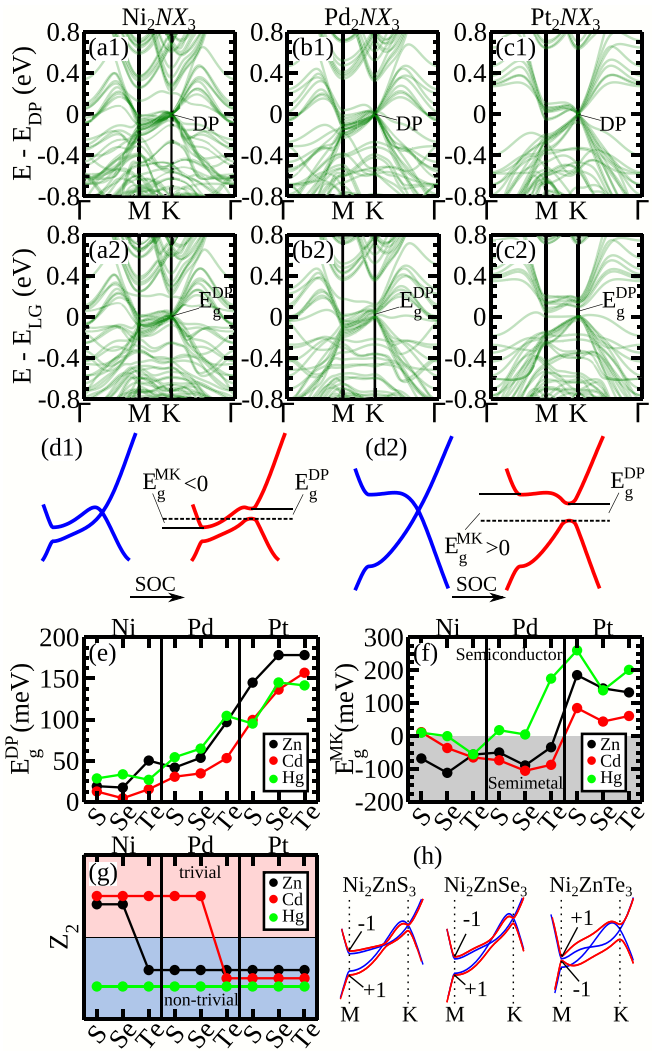

FIG. 2. Superposition of band structures for the (a) Ni_2NX_3, (b) Pd_2NX_3, and (c) Pt_2NX_3 systems, (a1)–(c1) without SOC and energy in relation to the DP (E_{DP}) and (a2)–(c2) with SOC and energy in relation to the K point gap's lower band (E_{LG}). (d) Depiction of the Dirac bands and SOC effect in the (d1) downward band bending at M and (d2) graphenelike. (e) Dirac point SOC energy gap (E_g^{DP}). (f) Global energy gap between M and K points (E_g^{MK}). (g) Topological invariant. (h) Topological transition for Ni_2ZnX_3 with blue (red) lines indicating the states without (with) SOC.

lower when compared with that of its counterpart (Pt_2HgSe_3) jacutingaite.

Once we have shown the feasibility of the energetically stable counterparts of jacutingaite, we focus on the electronic properties and topological phases of single-layer M_2NX_3 systems. As shown in Fig. 2(a)–2(c), we found the emergence of Dirac cones ruled by the hexagonal $N-M-N$ buckled lattice. The projection of the energy bands, near the Fermi level, reveals that the Dirac cones are mostly composed of the transition metal $N(s)$ orbitals hybridized with the host $M(d)$ orbitals, viz., Ni($3d$), Pd($4d$), and Pt($5d$). It is noticeable that, for a given host transition metal M, the electronic band structures share nearly the same features around the Fermi level. For instance, in Fig. 2(a) we present the superposition of the electronic band structures of Ni_2NX_3 with $N =$ Zn, Cd, and Hg, and $X =$ S, Se, and Te; similarly for Pd_2NX_3 and Pt_2NX_3, as shown in Figs. 2(b) and 2(c). Such a figure, where each material contributes with a translucent set of lines (band structure), allows us to identify similar features in the compounds characterized by darker regions (more details can be found in the Supplemental Material [35]). In the absence of SOC, the linear dispersion of the energy bands at the K and K′ points gives rise to the Dirac points (DPs) indicated as DP in Figs. 2(a1)–2(c1), whereas by turning on the SOC contribution we find energy gaps taking place at the DPs [E_g^{DP} in Figs. 2(a2)–2(c2)]. The SOC in the system is mostly given by the M atoms [26], and its strength is a quantitative indication of the stability of topological states. Here, it is worth highlighting that SOC-induced energy gaps at the DP [Fig 2(e)] are larger in Pt_2ZnX_3 compared with the ones of the other Pt_2NX_3 systems. For instance, Pt_2ZnX_3 (with $X =$ Se or Te) presents $E_g^{DP} \approx 178$ meV, being larger by 34 meV (23%) compared with that of jacutingaite and its counterpart Pt_2HgTe_3, both systems present $E_g^{DP} = 145$ meV. In particular, these findings can be understood by comparing the equilibrium geometries of the $N-Pt-N$ buckled hexagonal lattice; namely, Zn–Pt–Zn presents lower values of vertical buckling and Zn–Pt equilibrium bond length ($d_{MN} = 2.55$ Å) compared with the ones of Hg–Pt–Hg, $d_{MN} = 2.79$ Å, strengthening the Pt contribution to the Zn(s) Dirac bands. It is worth pointing out that larger values of E_g^{DP} in Pt_2ZnX_3 have been maintained even upon the use of hybrid functionals (HSE). Here we found $E_g^{DP} = 232$ and 242 meV for $X =$ Se and Te, both values larger than that obtained for jacutingaite, 222 meV (in Ref. [52] the authors obtained 218 meV using the same calculation approach).

Besides the energy gap induced by the SOC at the K/K′ points, downward bending of the upper Dirac band along the K–M direction leads to lower values of global gaps and eventually results in semimetallic systems. In Fig. 2(f) we show the energy difference between the lower point of the upper Dirac band at the M point and the top of the Dirac valence band at the K point [E_g^{MK} in Figs. 2(d1) and 2(d2)]. Negative values of E_g^{MK}, for $M =$ Ni and Pd systems, indicate that they are semimetallic. For $M =$ Pt, the SOC strength always overcomes the downward band bending, where the semiconducting character has been preserved. Focusing on the Pt_2NTe_3 systems, we found indirect energy band gaps of 133 and 61 meV for $N =$ Zn and Hg, respectively, while Pt_2HgTe_3 presented a direct energy gap ($E_g^{DP} < E_g^{MK}$) of 142 meV.

To characterize the topological phase of the M_2NX_3 systems we have computed the Z_2 [53] invariant by analyzing the parity of each band at the time-reverse invariant momenta (TRIM) and considering all bands below the upper Dirac bands fully occupied [54]. It is worth noting that the presence of semimetallic bands does not necessarily rule out the (possible) emergence of topologically nontrivial phases, characterizing a Z_2-metallic phase [55]. In this case, the edge states are no longer protected against backscattering processes. Our results, summarized in Fig. 2(g), reveal that, while all Hg compounds present a nontrivial topological phase, Ni_2ZnX_3 and Pd_2CdX_3 systems present a trivial → nontrivial topological transition for $X =$ S → Te. In these systems, there is an extra

crossing of the Dirac bands (without SOC) along the M-K path [blue lines in Fig. 2(h)], which causes a parity inversion from the original graphenelike bands. Such an inversion is overcome by the SOC, changing the parity order at the TRIM, for $X = \mathrm{Te}$ leading to the Z_2 nontrivial topological phase, whereas in Ni_2ZnX_3 the strength of the SOC is not enough to reinvert this extra crossing.

In addition to the topological phase control (trivial $\leftrightarrow$ nontrivial), as a function of the chemical composition in M_2NX_3 jacutingaitelike structures, other properties are worth examining in order to achieve technological applications, as well as integration with other 2D materials, for instance, the behavior of the SOC (nontrivial) energy gap as a function of the mechanical strain. Here, we found that the topological phase of the M_2NX_3 jacutingaitelike systems are robust against biaxial strain. In particular, for Pt_2ZnSe_3, there is an increase of the SOC-induced nontrivial energy band gaps, E_g^{DP}, from 178 to 185 meV upon a compressive strain of 2%. It reaches to ~194 meV in Pt_2ZnTe_3 compressed by 2.5%. Another key feature, in order to perform electronic engineering based on M_2NX_3 2D heterostructures [56], is the work function (Φ). By examining its dependence on the chemical composition, we found that for a given MX_2 host, Φ varies as a function of the foreign transition metal N. For instance, considering the $PtSe_2$ host, we found $\Phi = 4.90$ eV for jacutingaite ($N = \mathrm{Hg}$), and it decreases to about 4.70 eV in Pt_2ZnSe_3. Meanwhile, in Pt_2NTe_3, Φ reduces to 4.73 and 4.43 eV for $N = \mathrm{Hg}$ and Zn, respectively. Further details of the SOC-induced band gap as a function of biaxial strain and M_2NX_3 work functions can be found in the Supplemental Material [35].

In conclusion, we have shown that beyond jacutingaite, which is a naturally occurring mineral, there are other jacutingaitelike (M_2NX_3) structures that also host the Kane-Mele QSH phase. The energetic stability of these M_2NX_3 jacutingaite counterparts was thoroughly investigated, based on formation energy calculations combined with the recent convex hull analysis. We found that the M_2NX_3 structures are quite stable for chalcogenide (X) Se and Te atoms. Further calculations of the cleavage energies showed that these systems can be isolated in monolayers by commonly used exfoliation methods. The topological phases were characterized upon the calculation of Z_2 and Z_2-metallic invariants, where we found that for $N = \mathrm{Hg}$ the nontrivial phase was preserved for any combination between the transition metal M (= Ni, Pd, and Pt) and the chalcogenide atom X (= S, Se, and Te). In contrast, for the other foreign transition metals, $N = \mathrm{Zn}$ and Cd, the topological phase depended on the combination of the host (MX_2) atoms. Finally, we found that the Zn compounds, Pt_2ZnSe_3 and Pt_2ZnTe_3, present larger values of topological band gap compared with that of jacutingaite (Pt_2HgSe_3), while by changing the host element, $X = \mathrm{Se} \rightarrow \mathrm{Te}$, the band gap is practically the same; however, it becomes direct. Nevertheless, the presented class of materials introduces a family of compounds hosting the Kane-Mele topological phase, which can be of interest in device engineering.

The authors acknowledge financial support from the Brazilian agencies FAPESP (Grants No. 19/20857-0 and No. 17/02317-2), CNPq, and FAPEMIG, and they acknowledge the CENAPAD-SP and Laboratório Nacional de Computação Científica (LNCC-SCAFMat2) for computer time.

[1] M. Z. Hasan and C. L. Kane, Colloquium: Topological insulators, Rev. Mod. Phys. **82**, 3045 (2010).

[2] C. Mera Acosta, E. Ogoshi, A. Fazzio, G. M. Dalpian, and A. Zunger, The Rashba scale: Emergence of band anti-crossing as a design principle for materials with large Rashba coefficient, Matter **3**, 145 (2020).

[3] L. L. Tao and E. Y. Tsymbal, Persistent spin texture enforced by symmetry, Nat. Commun. **9**, 2763 (2018).

[4] X. Liang, X. Wu, J. Hu, J. Zhao, and X. C. Zeng, Large magnetic anisotropy in chemically engineered iridium dimer, Commun. Phys. **1**, 74 (2018).

[5] M. Jiang, H. Asahara, S. Sato, T. Kanaki, H. Yamasaki, S. Ohya, and M. Tanaka, Efficient full spin–orbit torque switching in a single layer of a perpendicularly magnetized single-crystalline ferromagnet, Nat. Commun. **10**, 2590 (2019).

[6] K. S. Novoselov, A. K. Geim, S. V. Morozov, D. Jiang, Y. Zhang, S. V. Dubonos, I. V. Grigorieva, and A. A. Firsov, Electric field effect in atomically thin carbon films, Science **306**, 666 (2004).

[7] E. C. Ahn, 2D materials for spintronic devices, npj 2D Mater. Appl. **4**, 17 (2020).

[8] K. Premasiri and X. P. A. Gao, Tuning spin-orbit coupling in 2D materials for spintronics: A topical review, J. Phys.: Condens. Matter **31**, 193001 (2019).

[9] A. Avsar, H. Ochoa, F. Guinea, B. Özyilmaz, B. J. van Wees, and I. J. Vera-Marun, Colloquium: Spintronics in graphene and other two-dimensional materials, Rev. Mod. Phys. **92**, 021003 (2020).

[10] C. L. Kane and E. J. Mele, Quantum Spin Hall Effect in Graphene, Phys. Rev. Lett. **95**, 226801 (2005).

[11] C. Si, K.-H. Jin, J. Zhou, Z. Sun, and F. Liu, Large-gap quantum spin Hall state in MXenes: d-band topological order in a triangular lattice, Nano Lett. **16**, 6584 (2016).

[12] N. C. Frey, H. Kumar, B. Anasori, Y. Gogotsi, and V. B. Shenoy, Tuning noncollinear spin structure and anisotropy in ferromagnetic nitride MXenes, ACS Nano **12**, 6319 (2018).

[13] W.-x. Ji, C.-w. Zhang, M. Ding, P. Li, and P.-j. Wang, Quantum spin Hall phase transitions in two-dimensional SbBi alloy films, J. Mater. Chem. C **5**, 2649 (2017).

[14] F. Reis, G. Li, L. Dudy, M. Bauernfeind, S. Glass, W. Hanke, R. Thomale, J. Schäfer, and R. Claessen, Bismuthene on a SiC substrate: A candidate for a high-temperature quantum spin Hall material, Science **357**, 287 (2017).

[15] S. Singh and A. H. Romero, Giant tunable Rashba spin splitting in a two-dimensional BiSb monolayer and in BiSb/AlN heterostructures, Phys. Rev. B **95**, 165444 (2017).

[16] C. Weeks, J. Hu, J. Alicea, M. Franz, and R. Wu, Engineering a Robust Quantum Spin Hall State in Graphene via Adatom Deposition, Phys. Rev. X **1**, 021001 (2011).

[17] H. Zhang, C. Lazo, S. Blügel, S. Heinze, and Y. Mokrousov, Electrically Tunable Quantum Anomalous Hall Effect in Graphene Decorated by 5*d* Transition-Metal Adatoms, Phys. Rev. Lett. **108**, 056802 (2012).

[18] C. M. Acosta, M. P. Lima, R. H. Miwa, A. J. R. da Silva, and A. Fazzio, Topological phases in triangular lattices of Ru adsorbed on graphene: *Ab initio* calculations, Phys. Rev. B **89**, 155438 (2014).

[19] I. I. Klimovskikh, M. M. Otrokov, V. Y. Voroshnin, D. Sostina, L. Petaccia, G. Di Santo, S. Thakur, E. V. Chulkov, and A. M. Shikin, Spin-orbit coupling induced gap in graphene on Pt(111) with intercalated Pb monolayer, ACS Nano **11**, 368 (2017).

[20] A. M. Afzal, K. H. Min, B. M. Ko, and J. Eom, Observation of giant spin-orbit interaction in graphene and heavy metal heterostructures, RSC Adv. **9**, 31797 (2019).

[21] T. Wakamura, F. Reale, P. Palczynski, M. Q. Zhao, A. T. C. Johnson, S. Guéron, C. Mattevi, A. Ouerghi, and H. Bouchiat, Spin-orbit interaction induced in graphene by transition metal dichalcogenides, Phys. Rev. B **99**, 245402 (2019).

[22] Z. Qiao, W. Ren, H. Chen, L. Bellaiche, Z. Zhang, A. H. MacDonald, and Q. Niu, Quantum Anomalous Hall Effect in Graphene Proximity Coupled to an Antiferromagnetic Insulator, Phys. Rev. Lett. **112**, 116404 (2014).

[23] Z. Wang, C. Tang, R. Sachs, Y. Barlas, and J. Shi, Proximity-Induced Ferromagnetism in Graphene Revealed by the Anomalous Hall Effect, Phys. Rev. Lett. **114**, 016603 (2015).

[24] J. B. S. Mendes, O. Alves Santos, L. M. Meireles, R. G. Lacerda, L. H. Vilela-Leão, F. L. A. Machado, R. L. Rodríguez-Suárez, A. Azevedo, and S. M. Rezende, Spin-Current to Charge-Current Conversion and Magnetoresistance in a Hybrid Structure of Graphene and Yttrium Iron Garnet, Phys. Rev. Lett. **115**, 226601 (2015).

[25] A. R. Cabral, H. F. Galbiatti, R. Kwitko-Ribeiro, and B. Lehmann, Platinum enrichment at low temperatures and related microstructures, with examples of hongshiite (PtCu) and empirical 'Pt_2HgSe_3' from Itabira, Minas Gerais, Brazil, Terra Nova **20**, 32 (2008).

[26] A. Marrazzo, M. Gibertini, D. Campi, N. Mounet, and N. Marzari, Prediction of a Large-Gap and Switchable Kane-Mele Quantum Spin Hall Insulator, Phys. Rev. Lett. **120**, 117701 (2018).

[27] J. I. Facio, S. K. Das, Y. Zhang, K. Koepernik, J. van den Brink, and I. C. Fulga, Dual topology in jacutingaite Pt_2HgSe_3, Phys. Rev. Mater. **3**, 074202 (2019).

[28] B. Ghosh, S. Mardanya, B. Singh, X. Zhou, B. Wang, T.-R. Chang, C. Su, H. Lin, A. Agarwal, and A. Bansil, Saddle-point Van Hove singularity and dual topological state in Pt_2HgSe_3, Phys. Rev. B **100**, 235101 (2019).

[29] A. Marrazzo, N. Marzari, and M. Gibertini, Emergent dual topology in the three-dimensional Kane-Mele Pt_2HgSe_3, Phys. Rev. Res. **2**, 012063 (2020).

[30] K. Kandrai, P. Vancsó, G. Kukucska, J. Koltai, G. Baranka, Á. Hoffmann, Á. Pekker, K. Kamarás, Z. E. Horváth, A. Vymazalová, L. Tapasztó, and P. Nemes-Incze, Signature of large-gap quantum spin hall state in the layered mineral jacutingaite, Nano Lett. **20**, 5207 (2020).

[31] I. Cucchi, A. Marrazzo, E. Cappelli, S. Riccò, F. Y. Bruno, S. Lisi, M. Hoesch, T. K. Kim, C. Cacho, C. Besnard, E. Giannini, N. Marzari, M. Gibertini, F. Baumberger, and A. Tamai, Bulk and Surface Electronic Structure of the Dual-Topology Semimetal Pt_2HgSe_3, Phys. Rev. Lett. **124**, 106402 (2020).

[32] A. Vymazalová, F. Laufek, M. Drábek, A. R. Cabral, J. Haloda, T. Sidorinová, B. Lehmann, H. F. Galbiatti, and J. Drahokoupil, Jacutingaite, Pt_2HgSe_3, a new platinum-group mineral species from the Cauê iron-ore deposit, Itabira district, Minas Gerais, Brazil, Can. Mineral. **50**, 431 (2012).

[33] R. Longuinhos, A. Vymazalová, A. R. Cabral, S. S. Alexandre, R. W. Nunes, and J. Ribeiro-Soares, Raman spectrum of layered jacutingaite (Pt_2HgSe_3) crystals—Experimental and theoretical study, J. Raman Spectrosc. **51**, 357 (2020).

[34] F. Laufek, A. Vymazalová, and M. Drábek, Powder diffraction study of Pd_2HgSe_3, Powder Diffr. **32**, 244 (2017).

[35] See Supplemental Material at http://link.aps.org/supplemental/10.1103/PhysRevB.102.235153 for (i) computational details, (ii) ternary phase diagram, (iii) phonon dispersion of Pt_2ZnTe_3, (iv) detailed band structures, (v) strain effect on the SOC gap, and (vi) work function.

[36] G. Kresse and J. Furthmüller, Efficiency of ab-initio total energy calculations for metals and semiconductors using a plane-wave basis set, Comput. Mater. Sci. **6**, 15 (1996).

[37] J. P. Perdew, K. Burke, and M. Ernzerhof, Generalized Gradient Approximation Made Simple, Phys. Rev. Lett. **77**, 3865 (1996).

[38] J. Heyd, G. E. Scuseria, and M. Ernzerhof, Hybrid functionals based on a screened Coulomb potential, J. Chem. Phys. **118**, 8207 (2003).

[39] J. Heyd, G. E. Scuseria, and M. Ernzerhof, Erratum: Hybrid functionals based on a screened Coulomb potential [J. Chem. Phys. **118**, 8207 (2003)], J. Chem. Phys. **124**, 219906 (2006).

[40] H. J. Monkhorst and J. D. Pack, Special points for Brillouin-zone integrations, Phys. Rev. B **13**, 5188 (1976).

[41] P. E. Blöchl, Projector augmented-wave method, Phys. Rev. B **50**, 17953 (1994).

[42] K. Lee, É. D. Murray, L. Kong, B. I. Lundqvist, and D. C. Langreth, Higher-accuracy van der Waals density functional, Phys. Rev. B **82**, 081101(R) (2010).

[43] A. Jain, S. P. Ong, G. Hautier, W. Chen, W. D. Richards, S. Dacek, S. Cholia, D. Gunter, D. Skinner, G. Ceder, and K. A. Persson, Commentary: The Materials Project: A materials genome approach to accelerating materials innovation, APL Mater. **1**, 011002 (2013).

[44] L. Chaput, A. Togo, I. Tanaka, and G. Hug, Phonon-phonon interactions in transition metals, Phys. Rev. B **84**, 094302 (2011).

[45] A. Togo and I. Tanaka, First principles phonon calculations in materials science, Scr. Mater. **108**, 1 (2015).

[46] S. P. Ong, L. Wang, B. Kang, and G. Ceder, Li-Fe-P-O_2 phase diagram from first principles calculations, Chem. Mater. **20**, 1798 (2008).

[47] S. P. Ong, A. Jain, G. Hautier, B. Kang, and G. Ceder, Thermal stabilities of delithiated olivine MPO4 (M = Fe, Mn) cathodes investigated using first principles calculations, Electrochem. Commun. **12**, 427 (2010).

[48] G. R. Schleder, C. M. Acosta, and A. Fazzio, Exploring two-dimensional materials thermodynamic stability via machine learning, ACS Appl. Mater. Interfaces **12**, 20149 (2020).

[49] $\delta = (E_{\text{bulk}} - E_{\text{ML}})/A$, where E_{bulk} (E_{ML}) is the total energy of the bulk (monolayer) system and A is the monolayer of the unity cell area.

[50] K. Choudhary, I. Kalish, R. Beams, and F. Tavazza, High-throughput identification and characterization of two-dimensional materials using density functional theory, Sci. Rep. **7**, 5179 (2017).

[51] W. Wang, S. Dai, X. Li, J. Yang, D. J. Srolovitz, and Q. Zheng, Measurement of the cleavage energy of graphite, Nat. Commun. **6**, 7853 (2015).

[52] X. Wu, M. Fink, W. Hanke, R. Thomale, and D. Di Sante, Unconventional superconductivity in a doped quantum spin Hall insulator, Phys. Rev. B **100**, 041117(R) (2019).

[53] C. L. Kane and E. J. Mele, Z_2 Topological Order and the Quantum Spin Hall Effect, Phys. Rev. Lett. **95**, 146802 (2005).

[54] L. Fu and C. L. Kane, Topological insulators with inversion symmetry, Phys. Rev. B **76**, 045302 (2007).

[55] B. Zhao, J. Zhang, W. Feng, Y. Yao, and Z. Yang, Quantum spin Hall and Z_2 metallic states in an organic material, Phys. Rev. B **90**, 201403(R) (2014).

[56] A. K. Geim and I. V. Grigorieva, Van der Waals heterostructures, Nature (London) **499**, 419 (2013).